3.2.2. Numerical Simulation and Experimental Validation of Supersonic Systems

Kazuhiko Sakaki

Shinshu University, Faculty of Engineering

3.2.2.1. Introduction

Calculation and optimization of thermal spraying nozzles geometry is known to be a key issue of spraying equipment development. The advanced supersonic spraying equipment such as High velocity oxygen-fuel (HVOF) thermal spray and cold spray (CS) systems being developed over the last decade are the main representatives using De Laval nozzles. The fields of application of the HVOF and CS spraying technologies are expanding rapidly. That is why calculation and optimization of thermal spraying nozzles geometry are of great importance.

One of the major characteristics of the HVOF process is the high-speed gas jet, which is governed by gas dynamics. In gas dynamics, supersonic flows are obtained with convergent-divergent nozzle, which are used for rocket motors. Rocket motors, including their nozzle design, have been studied and analyzed in detail. While the principal purpose of the design of a rocket motor nozzle is to maximize the thrust, in thermal spraying the main purpose is to obtain better coating quality.

The HVOF systems employ various kinds of gun nozzle contours, such as convergent-barrel (Mason et al.. 1984[1)], Kowaisky et al.. 1990[2)]) convergent-divergent (or de Laval nozzle) (Diamond Jet 1995[3)]), convergent-multi-stage divergent (Carbide Jet System 1995[4)]) and convergent-divergent-barrel (Thope et al.. 1992[5)], Heath et al.. 1998[6)]). The HVOF gun systems without any nozzle are also in use (Diamond Jet 1995[3)]).

Previous studies on thermal spraying show that the coating properties are principally determined by the thermal and kinetic energy states of particles upon impact with the substrate. In order to have a balance between these two states; various changes in the design of the HVOF gun nozzle have been attempted. However, the works concerning the influence of nozzle geometry on the thermal spray process are sparse (Hackette et al.. 1995[7)], Sakaki et al.. 1998[8)], Kopiola et al.. 1997[9)]).

Previously, we have considered the effect of throat diameter and exit divergence of the gun nozzle on the HVOF process (Sakaki et al.. 1998[8)], Sakaki et al.. 1997[10)], Sakaki et al.. 1998[11)]). The combustion gas flow (such as pressure, velocity, temperature, and expansion state of gas jet from the nozzle exit), the particle behavior, and, therefore, the nature of the coatings were found to be significantly influenced by these nozzle parameters. In addition, the effect of the expansion state of the combustion gas jet on

the HVOF process was investigated using a diverging nozzle exit. The particle velocity reached a maximum with the correct expansion state of the gas jet due to an increased gas jet velocity. This resulted in an increase in the bonding strength of the NiCrAlY coating (Sakaki et al. 1999[12)]).

In the present Chapter, the effect of increasing the length of the entrance convergent section of the nozzle on HVOF thermal spraying process has been investigated by a numerical simulation and experiments with a Jet Kote^{TM} system (Stellite Coatings, Goshen, IN). The gas flow in the entrance convergent section of the nozzle is of relatively higher temperature and is subsonic; therefore, this region will be convenient for heating of the high-melting-point spray materials such as ceramics and refractory metals. The goal of this analysis is to establish a design for the HVOF gun nozzle in order to gain better coating quality of any material powder.

The nozzle geometry is also important with regard to the cold spray method (Bhhgat et al. 1997[13)]). In the cold spray method, a coating is formed by exposing a substrate to high velocity solid-phase particles, which have been accelerated by supersonic gas flow at a temperature much lower than the melting or softening temperature of the feedstock. The effect in HVOF process will also be applied to the

nozzle design for the cold spray method. The influence of nozzle geometry and gas initial conditions on the cold spray process (*i.e.*, the behavior of the carrier gas and spray particles) within the nozzle is investigated by a numerical simulation prior to designing the cold spray equipment and producing coatings.

3.2.2.2. Equipment and Methods

HVOF Thermal Spray Equipment

The Jet Kote^{TM} HVOF thermal spray system with a mass-flow-controller attachment was used for the present study. A schematic diagram of the Jet Kote^{TM} gun and nozzle are shown in Fig.3.21. Propylene, C_3H_6, gas was used as the fuel and the spray conditions used are given in Table 3.5. Some technical characteristics of this system are: (1) employs an internal combustion chamber to generate the hot, extreme velocity exhaust jet to spray, and (2) injects powder axially into the center of the exhaust gas jet at the nozzle intake. In this system, combustion gas flows from the combustion chamber through four holes in the combustion head (changing its direction at a right angle) to the nozzle intake with an initial velocity of U_{gi}.

Fig.3.21. Schematic diagram of HVOF (JetKote ^{TM}) spraying gun and nozzle

Table 3.5 HVOF spraying parameters and initial condition

In order to study effects of the gun nozzle geometry, on the combustion gas behavior, spray particles, and coating properties, two different nozzle shapes, namely a “straight nozzle” (equal to factory standard-made barrel one) and a “convergent nozzle” were used for the present study. Further, the dimensions such as total length l of the straight nozzle and convergent length $l_{conv.}$ at the entrance of the convergent nozzle were varied, as shown in Table 3.6. The length l of a straight nozzle (in the following, straight nozzle is indicated by “total nozzle length l –S.”) was varied to three different levels namely 76.5mm(3in.), 156.2mm(6in.) and 304.8mm(12in.). A convergent nozzle (in the following, the converging nozzle is indicated by “l –length of entrance convergent part $l_{conv.}$ Conv.”) was made by increasing the $l_{conv.}$ of straight-nozzle shown in Fig.3.22. The throat diameter d_t and exit diameter d_e were fixed at 7.8mm.

Table 3.6 Shape and size of gun nozzle used and state of combustion gas stream

Fig.3.22. Conceptual drawing of the cold spray equipment

Thermal spray powder

NiCrAlY alloy powder of Ni-13Cr-5Al-0.5mass%Y composition (SHOCOAT^{R} MA-90, gas atomized powder (Showa Denko, Tokyo) was used for the present study.

An increase in the entrance part of the nozzle can cause an increase in the heat input of particles and oxidize NiCrAlY particles. Therefore, Al_2O_3-40mass%TiO_2 powder (Shocoat^R K-40F, crushed powder) was also used. Properties of these powders are shown in Table 3.7.

Table 3.7 HVOF spraying powder properties

Evaluation approach

The expansion state of HVOF jets from the gun nozzle exit with nozzles used without spray powder were evaluated by means of visual observation and by photographic methods. The nozzle intake pressure was measured through a powder feed port by a pressure indicator (PF-30KF, Kyowa Electronic Instrument, Tokyo).(Sakaki et al.1997[10]). The velocity, surface temperature, and diameter of the sprayed particles during HVOF spraying were measured using an in-flight particle measurement system; namely the DPV-2000 (Tecnar Automation Ltd. , St-Bruno, QC, Canada), which detects the thermal radiation emitted by hot in-flight-particles (Gougeon et al. 1994[14]).

The nature of sprayed coatings was characterized by means of electron probe microanalysis (EPMA), micro-hardness, and X-ray diffraction analysis.

The deposition efficiency was ascertained by measuring the weight gains on mild steel substrates of 75×105×6mm dimensions for a spray time of 30s taking into account the known feedstock powder flow rate.

3.2.2.3. Numerical simulation of thermal spray process

HVOF process

There are several techniques that can be used to calculate the gas flow of HVOF systems. Recent analyses have used CFD methods to simulate this complex phenomenon in two dimensions. In the present paper, the internal nozzle flow was treated as quasi-one-dimensional isentropic flow. This one-dimensional approximation is simple and sufficiently correct for the present purpose of expressing an effect of nozzle geometry on the internal nozzle flow (Sakaki et al. 1997[10]). Detailed derivation of the modeling can be found in (Sakaki et al.1997[10]) and (Sakaki et al. 1998[11]). A brief description of the simulation is given bellow.

Modeling of combustion gas flow within the nozzle. The following assumptions were made to model the gas flow in the HVOF gun nozzle (Sakaki et al. 1997[10]):

- Combustion gas flow within the nozzle is the quasi-one-dimensional isentropic flow of semi-perfect gas.

- The chemical reaction of combustion in the combustion chamber follows as Eq.(3.4) so that combustion gas is composed only of CO_2, H_2O (gas), excessive O_2, and carrier gas N_2.

$$C_3H_6+(9/2+X)O_2+YN_2=3CO_2+3H_2O+XO_2+YN_2+1926[kJ/mol] \quad (3.4)$$

- Combustion gas flows from the combustion chamber to the nozzle intake with an initial velocity Ug_i, temperature Tg_i, and pressure P_i.
- Principles of heat transfer only apply to heat exchange between the hot combustion gas and combustion chamber wall/ cooling water.

In this manner, the pressure P, density ρg, temperature Tg, and velocity Ug of the gas flow can be calculated from the ratio of the nozzle cross-sectional area at a given point to the nozzle throat area (Matuo1994[15]).

Modeling of particle behavior within the nozzle. Particle acceleration and heating in a gas flow within the nozzle are given by solving the equations of motion and heat transfer as described below. These equations in the present paper are based on the following four assumptions.

- The spray particle is spherical with negligible internal temperature gradients.

- The particle specific heat is independent of its temperature and constant.
- The gravitational effect and the interaction between particles are ignored.
- The influences of particles on gas flow are neglected. This is equivalent to stating that the gas energy decrease along the nozzle due to acceleration and heating of the particle is neglected.

Under the above assumptions, the equations of motion of a particle in the HVOF process can be written as

$$\frac{dU_p}{dt} = \frac{3}{4}\frac{C_d}{D_p}\frac{\rho_g}{\rho_p}\left(U_g - U_p\right)\left|U_g - U_p\right| \tag{3.5}$$

, where U_p is the particle velocity, t is time, C_d is the drag coefficient, D_p is the particle diameter, ρ_g is the combustion gas density, ρ_p is the particle density, and U_g is the gas velocity. C_d for sphere is function of particle Reynolds number (Clift et al.. 1987[16]).

Heating of a particle in a gas flow can be expressed as follows:

$$\frac{dT_p}{dt} = \left(T_g - T_p\right)\frac{6h}{c_p\rho_p D_p} \tag{3.6}$$

, where T_p is the particle temperature, T_g is gas temperature, h is the heat transfer coefficient, and c_p is the specific heat of particle. The heat transfer coefficient h in Eq.(3.6) can be found by means of the semi-empirical Ranz-Marshall equation, in

which h is a function of the Reynolds number and the Prandtl number. The influence of radiant heat between the combustion gas and particle was neglect.

For the calculation of the Reynolds number and the Prandtl number, the values of the specific heat of gas, the gas viscosity, and the gas thermal conductivity are used in the film temperature T_f, which is defined by (JSME Handbook 1993[17]).

$$T_f=(T_g+T_p)/2 \qquad (3.7)$$

When T_p reaches the melting point of the particle T_{mp}, the heat from the gas to particle, Q, will be the heat of fusion of the particle. The particle state is represented by the degree of melting of the particle as follows:

$$\frac{\sum Q}{Q_f}=\frac{h\int(T_g-T_{mp})dt}{\rho_p D_p L} \qquad (3.8),$$

where Q_f is heat of fusion per particle and L is latent heat of fusion of particle material.

Numerical Approximation of the HVOF process. An outline of a numerical approximation of the HVOF process is as follows: (1) initial conditions were given, (2) the pressure P, the temperature T_g, and the velocity U_g of the gas flow were calculated from the ratio of the cross-sectional area of the nozzle at the intake point to the nozzle throat area;(3) the above differential equations Eq.(3.5 and 3.6) concerning

particle behavior were solved numerically by the Euler method; and (4) the process of (2) and (3) were repeated from nozzle the intake to the nozzle exit.

The thermal spray condition data and the initial conditions shown in Table 3.5 (except the powder feed rate and the spray distance) were used. Values of diameter, density, melting point, specific heat, and latent heat of fusion of spray power used in calculation are given in Table 3.7.

The results provided by this simulation could be a little larger than the real values because of the above assumptions.

Cold spray process

A conceptual drawing of the cold spray equipment for the present study is shown in Fig.3.22. Compressed nitrogen gas is introduced to a heater and a powder feeder. The pressure gas is heated in an electric furnace. Feedstock powder is injected axially and centrally into the gas flow at the gun nozzle intake. The spray gun is fitted with a convergent-divergent nozzle (or a conical de Laval nozzle) designed to produce a correct expansion gas jet (Sakaki et al.., 1998[8)]), which is supersonic at its exit, and free shock diamonds. Namely, the nozzle exit pressure P_e of the gas fed at varied nozzle

intake pressures P_i matches the ambient pressure by changing exit diameter d_e. The total nozzle length l and throat diameter $d_t$is fixed at 300mm and 5mm, respectively. Spray powder used in this study is Ni-Al bronze since prior studies (Bhhgat et al.. 1997[13]) have created a coating with this powder by cold spray method. Alkimov*et al.* have reported that there exists a critical velocity U_{pcr} for each coating and substrate material combination, above which the particles have sufficient kinetic energy to build a coating (Alkhimov et al.. 1990[18]). The value of U_{pcr} for a Ni-Al bronze particle in the present study is 600m/s, because typical values of U_{pc} for copper, zinc, nickel, and iron range from 550 to 650m/s for a copper substrate. (Alkhimov et al.. 1990[18])

The spray parameters used in this simulation are shown in Table 3.8. The basic treatment for the cold spray simulation is the same as that for HVOF simulation. The same assumptions as applied to the HVOF process were made to model the cold spray process with an additional one that the gas flow within the nozzle is the quasi-one-dimensional isentropic flow of semi-perfect gas.

Table 3.8. Initial conditions of cold spray process simulation

The equations of motion and heating of a particle in the cold spray process can be written as Eq.(3.5 and 3.6) under above the assumptions. An important distinction between the modeling of the two processes is that the influence of radiant heat of the

gas on the particle might be neglect, since the gas temperature was lower. The numerical approximation of the cold spray process and of the HVOF process are basically, the same.

3.2.2.4. Validation of the Numerical Simulation

3.2.2.4.1 Effect of Convergent Section Length on the HVOF Spraying Process

The numerical simulation results on the effect of increasing the nozzle entrance convergent section length l_{conv} on gas velocity U_g, temperature T_g, particle velocity U_p, and other properties are given in Fig.3.23 and as part of Table 3.6. The results show that the gas flow in the entrance convergent section of the nozzle is of a higher relative temperature and subsonic. Therefore, the degree of particle melting Q/Q_L increases and U_p decreases slightly with increasing l_{conv}. The calculated U_{pe} agreed approximately with the values measured by the in-flight particle measurement system for NiCrAlY HVOF processes in change with l_{conv}. This tendency was confirmed by observing the nature of the sprayed coatings; namely, cross-section hardness and oxygen content of NiCrAlY coatings increase and deposition efficiency decreases with increasing l_{conv}. As an example of the effect of increasing in l_{conv} on the coating property, surface structures of Al_2O_3-40mass%TiO_2 coatings are shown in

Fig.3.24, in which coatings sprayed with a longer nozzle by HVOF and by plasma spray are compared.

Fig.3.23. Effect of increasing the length of the nozzle entrance convergent section (for three nozzle shapes) with calculated results of the (a) nozzle contour, (b)gas pressure, (c)velocity of gas and particle, (d)particle resident time, and (e)temperature of gas and particles and the degree of melting particle

Fig.3.24. Surface SEM structures of Al_2O_3-40mass%TiO_2 coatings sprayed by HVOF (with several nozzle shape) and plasma spraying. 3S. is 3in. straight nozzle, 3-26Conv. is 3in. converging nozzle with 26mm converging part length, 3-48Conv. is 3in. converging nozzle with 48mm converging part length, 6S. is 6in. straight nozzle, 12S. is 12in. straight nozzle

It was found that splat morphologies vary with l^{conv} and nozzle length l, because input heats of particles from the gas or degree of melting increase with increasing l^{conv} and l.

Figure 3.25 shows some typical the structure of Al_2O_3-40mass%TiO_2 splats sprayed by HVOF and collected on 304 stainless steel substrates at room temperature. In order to obtain isolated splats, a shielding plate on which several holes of 1 mm were distributed was placed parallel to the substrate at a distance of about 5mm. The splat patterns are roughly divided into the following three categories: (a) non-molten particles, (b) semi-molten particles, and (c) molten particles with splash. The different morphologies arise due to variations in the input heat of particles, substrate

temperature and impact velocity of particle to substrate. From (a) to (c), the input heat of particles increases.

Fig.3.25. Typical patterns of the structure of Al_2O_3-40mass%TiO_2 splats sprayed by HVOF collected on 304 stainless steel substrate: (a) of non-molten particle with trusting, (b) of semi-molten particle, and (c) of molten particle with splash.

The proportion of the various splat patterns of Al_2O_3-40mass%TiO_2 powder with respect to a change in the nozzle entrance convergent section length l_{conv} is shown in Fig.3.26. In this figure, the percentage of splat morphology (b) semi-molten particles and (c) molten particles with splash increase slightly with l_{conv} at three 76.2mm (3in.) nozzles (from 3S., 3-26Conv to 3-48Conv nozzle). This tendency shows that an increase in l_{conv} causes an increase in the gas input heat of particle.

Fig.3.26. Parentage of patterns of the structure of Al_2O_3-40mass%TiO_2 splats sprayed by HVOF with change in nozzle shape. 3S. is 3in. straight nozzle, 3-26Conv. is 3in. converging nozzle with 26mm converging part length, 3-48Conv. is 3in. converging nozzle with 48mm converging part length, 6S. is 6in. straight nozzle, 12S. is 12in. straight nozzle

Figure 3.27 shows the results of the deposition efficiency, the calculated degree of melting of particles, and the cross-section hardness of Al_2O_3-40mass%TiO_2 coatings with respect to a change in l_{conv} and total nozzle length l. The figure shows an increase in deposition efficiency and coating hardness with an increase in l_{conv}. Moreover, the deposition efficiency and the cross-section hardness of the coating with 3-48Conv nozzles are higher than those with longer nozzles such as 12S and 6S. This result can

be explained from heat losses by nozzle cooling and pipe fraction loss, which were observed in terms of the expansion state of the gas jet shown in Table 2. Therefore, these losses increase with the nozzle length, so that velocity and temperature of the gas and particles decreases with an increase in the nozzle length.

Fig.3.27. Effect of nozzle shape on (a) deposition efficiency, (b) degree of melting of particle and (c) cross-sectional hardness of sprayed Al_2O_3-40mass%TiO_2 coatings

In summary, the effect of increasing the length of the entrance convergent section of the particle-heating nozzle is larger than that of increasing the length of the barrel part or total nozzle length in the HVOF thermal spraying process. Therefore, a combination of increasing entrance convergent section length and total length of nozzle is more effective.

3.2.2.4.2 Influence of Gas Parameters and Nozzle Geometry on the Cold Spray Process

Influence of Particle Diameter.

The numerical simulation results (gas velocity U_g, temperature T_g, particle velocity U_p, and temperature T_p) with a change in the particle diameter of Ni-Al-bronze powder are given in Fig.3.28. The entrance convergent length $l_{conv.}$ of the conical de Laval nozzle used is 9mm, and the following initial conditions are used as baseline

conditions: gas pressure of 2.0 MPa(abs), temperature T_{gi} of 750K, and velocity U_{gi} of 0m/s, particle temperature T_{pi} of 300K, and velocity U_{pi} of 10m/s.

Fig.3.28. Numerical simulation results with a change in particle diameter of Ni-Al-bronze powder by cold spray: (a) velocity of gas and particle and (b) temperature of gas and particle (baseline: P_i=2MPa, U_{gi}=0m/s, T_{pi}=750K, U_{pi}=10m/s, and T_{pi}=300K)

Using the conical de Laval (convergent-longer divergent) nozzle, the gas velocity U_g increases along the axial distance within the nozzle to reach 950 m/s (Mach number M of 2.7) at the nozzle exit, and the gas temperature decreases to reach 290K(which is equal to room temperature).

Figure 3.28 shows that the particles, even the larger ones, are accelerated and heated very quickly. The results indicated that 20μm and smaller particles reach the critical velocity of 600m/s before arriving at the nozzle exit and attain the gas temperature within the entrance convergent part of the nozzle.

The value of T_g becomes lower than T_p in the nozzle, because the heat capacity of the gas is much lower than that of particle and the gas initial temperature was much lower. In conventional thermal spray processes such as HVOF, plasma spray, and so on, using higher temperature gas, this tendency is not observed.

Fig. 10
Fig. 11

Influence of Gas Initial Conditions.

Figure 3.29 shows the effect of initial gas pressure P_i on the cold spray process (velocity of gas U_{ge} and particle U_{pe} , temperature of gas T_{ge}, and particle T_{pe} at nozzle exit) with nozzles designed to produce a perfect expansion gas jet according to P_i. In the figure, U_{ge} and U_{pe} increase with an increase in P_i. Particles 20μm and smaller reach the critical velocity U_{pcr} at P_i above 2MPa. However, 50μm and larger particles cannot attain this velocity at P_i up to 5MPa. The value of T_{ge} and T_{pe} decrease with increasing P_i. For example, T_{ge} at P_i of 5MPa drops to 200 K (or –73□).

Fig.3.29. Effect of gas initial pressure on calculated results of cold spray process: (a) velocity of gas and Ni-Al bronze particle and (b) temperature of gas and particle (U_{gi}=0m/s, T_{gi}=750K, U_{pi}=10m/s, and T_{pi}=300K)

The effect of gas initial temperature T_{gi} on the cold spray process under the baseline conditions, except for $T_{gi,}$ is provided Fig.3.30. At most, the gas for cold spray might be used at a temperature up to 1000K. In this figure, the results up to 2500K are shown in order to compare with the results of the HVOF process. The value of U_{ge} and U_{pe} increase with T_{gi}. The Value of U_{pe} is higher than U_{pcr} at T_{gi} above 700K. It is clear that the minimum T_{gi} exists for these initial gas pressures, which allow particles to reach U_{pcr}. For the HVOF process, the pressure of the combustion gas is lower than that of the cold spray gas because the temperature of the combustion gas is much higher.

Fig.3.30. Effect of gas initial temperature on calculated results of cold spray process: velocity of gas and Ni-Al bronze particle(20μm), temperature of gas and particle (P_i=2MPa, U_{gi}=0m/s, U_{pi}=10m/s, and T_{pi}=300K).

The effect of the initial gas velocity, U_{gi}, on the cold spray process under the baseline conditions except, for U_{gi}, is indicated in Fig.3.31. With an increase in U_{gi},U_{ge} and U_{pe} increase slightly, while T_{ge} and T_{pe} decrease slightly. To heat powder effectively, gas might be supplied to the nozzle at lower velocity. However, particle behavior is independent of the gas initial velocity up to 100m/s.

Fig.3.31.Effect of gas initial velocity on calculated results of cold spray process: velocity of gas and Ni-Al bronze particle (20μm), temperature of gas and particle (P_i=2MPa, T_{gi}=750K, U_{pi}=10m/s, and T_{pi}=300K).

Influence of the Nozzle Entrance Convergent Section length.

The effect of increases the nozzle entrance convergent section length, $l_{conv.}$, on the cold spray process under the baseline conditions is given in Fig.3.32. The Value of T_{pe} increase steadily and T_{ge} increases slightly, while U_{pe} decreases steadily and U_{ge} decrease slightly with increasing $l_{conv.}$. Therefore, increasing $l_{conv.}$ affects particle heating but does not accelerate it in the same fashion as for as HVOF. Thus, l_{conv} must be up to 100mm under these spray conditions to obtain a critical velocity of 600m/s. However, now the influence of particle and substrate temperatures on the critical

velocity is not revealed. Increasing l_{conv} in order to lower the critical velocity can raise the particle temperature.

Fig.3.32. Effect of length of nozzle entrance convergent part on calculated results of cold spray process: velocity of gas and Ni-Al bronze particle (20μm), temperature of gas and particle (baseline: P_i=2MPa, U_{gi}=0m/s, T_{pi}=750K, U_{pi}=10m/s, and T_{pi}=300K)

3.2.2.5.Conclusion

Numerical simulation and experiments have investigated the effect of increasing the nozzle entrance converging section on the HVOF process. The numerical simulations also investigate this effect with regard to the spray parameters of the cold spray process. The results are summarized as follows.

- The particle temperature or the degree of melting of particles increase, but the particle velocity decreases slightly with an increase in the entrance convergent section length of the nozzle of HVOF and cold spray equipment. Therefore, increasing this length has an effect on particle heating.
- The surface structure and morphology of the splat pattern of Al_2O_3-40mass%TiO_2 coatings sprayed by HVOF vary with an increase in the nozzle entrance convergent section length.

- Deposition efficiency and cross-sectional hardness of Al_2O_3-40mass%TiO_2 coatings sprayed by HVOF significantly increase with the nozzle entrance convergent section length.
- In cold spray, gas velocity increases along the axial distance within the nozzle to reach 950 m/s (Mach number of 2.7) at the de Laval nozzle exit and gas temperature decreases to 290 K under the baseline initial conditions; gas pressure of 2.0 MPa (abs), temperature of 750 K, velocity of 0 m/s and particle temperature of 300 K and velocity of 10 m/s. Ni-Al bronze particles 20 μm and smaller reach the critical velocity.
- Initial gas pressure and temperature affect accelerating particles in the cold spray process. The initial gas velocity has a slight influence.

References

1. Mason, D. L. and Rao, K., in *Thermal Spray Coatings - New materials, Processes and Applications*, Longo, F. N. ed., American Society for Metal., Material Park, OH, 1984, 51-63.
2. Kowaisky, K. A., Marantz, D. R.,Smith, M. F. and Oberkampf,W. L., in *Thermal Spray Research and Applications*, Bernecki, T.F. ed., ASM International, Material Park, OH, 1990, 587-592.
3. *Product catalogue DIAMOND Jet*, SULZER METCO (US) Inc., New York, NY, 1995.
4. *Product catalogue Carbide Jet System (CJS)*, OZU-Mashinenbau GmbH, Castrop-Rauxel, Germany, 1995.

5. Thope, M.L. and Richer, H.J. ,in *Thermal Spray: International Advances in Coating Technology*, C.C.Bernt, ed., ASM International, Material Park, OH, 1992, 137-147.
6. Heath,G.R. and Dumola, R.J., in *Thermal Spray: Meeting the Challenges of 21st Century*, Coddet, C. ed., ASM International, Material Park, OH, 1998, 1495-1500.
7. Hackette, C. M. and Settles, G. S., *in Thermal Spray Science & Technology*, Berndt, C. C. and Sampath, S. ed., ASM International, Material Park, OH, 1995, 135-140.
8. Sakaki, K., Shimizu ,Y., Gouda, Y. and Devasenapathi, A., in *Thermal Spray: Meeting the Challenges of 21st Century*, Coddet, C., ed., ASM International, Material Park, OH, 1998, 445-450.
9. K.Kopiola, J.P.Hirvonen, L.Laas and F.Rossi:*J. of Thermal Spray Technology*, 1997, vol6(4), pp.469-474.
10. Sakaki, Shimizu,Y. , SAITOH, N. and Gouda, Y. ,*J. of Japan Thermal Spraying Soc.* , 1997, 34(1),1-9 (in Japanese).
11. Sakaki, K. , Shimizu ,Y., Y. Gouda and T. Minamida :*J. of Japan Thermal Spraying Soc.* , 1998, 35(3), 195-203 (in Japanese).
12. Sakaki, K. , Shimizu ,Y. and Y. Gouda :*J. of the Japan Institute of Metal..s*, 1999, 63(2), 269-76 (in Japanese).
13. Bhhgat, R.B., Amateau, M.F., Papyrin, A., Conway, J.C. ,.Stutaman, Jr., B and Jones, B., *in Thermal Spray: A United Forum for Science and Technological Advances*, Berndt, C.C. ed., ASM International, Material Park, OH, 1997, 361-367.
14. Gougeon, P., Moreau, C., Lacasse, V., Lamontage, M., Powell, I. and Bewsher, A., *Adv. Processing Tech. Particulate Mater.* , 1994, vol.6, 199-210.
15. For example, Matuo, K.: *Compressible Fluid Dynamics*, Rikougakusha, Tokyo,1994, 83(in Japanese).
16. Clift, R., Grace, J. R. and Weber, M. E., *Bubbles, Drops and Particles*, Academic Press, New York, NY ,1987.
17. *JSME Heat Transfer Handbook*, Japan Society of Mechanical Engineers, Tokyo, 1993, 44, (in Japanese).
18. Alkhimov, A.P., Kosarev, V.F. and Papyrin, A.N., *Dokl. Akad. Nauk USSR*, 1990, vol. 315, 1062-1065 (in Russian).

Figure captions

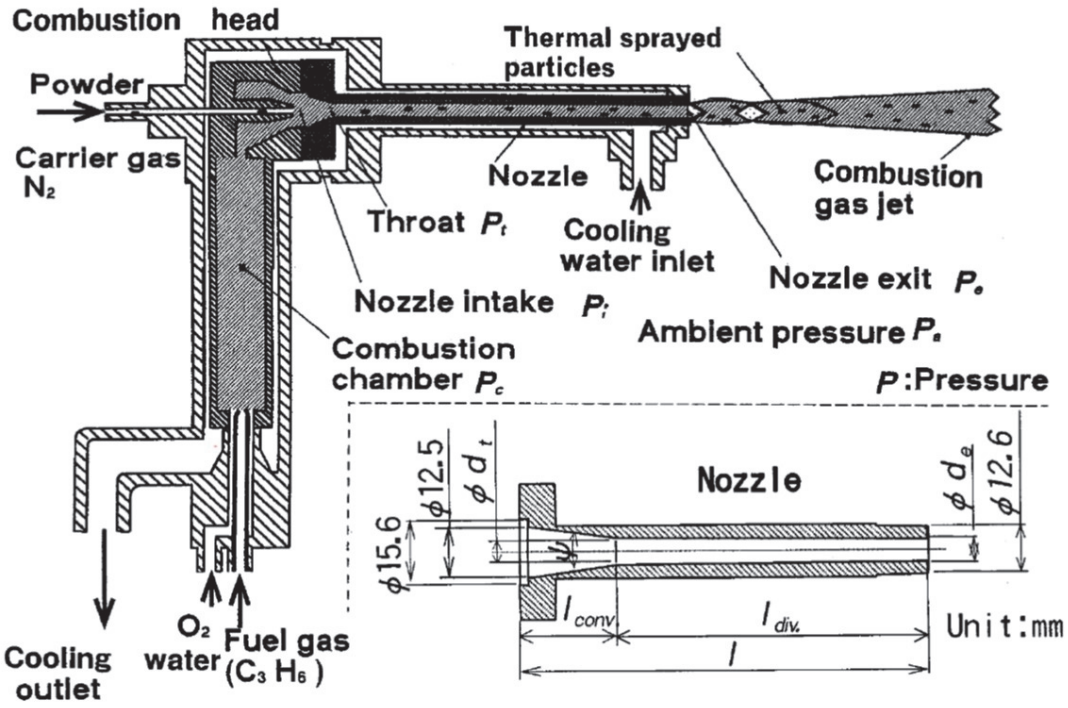

Fig.3.21. Schematic diagram of HVOF (Jet Kote ™) spraying gun and nozzle

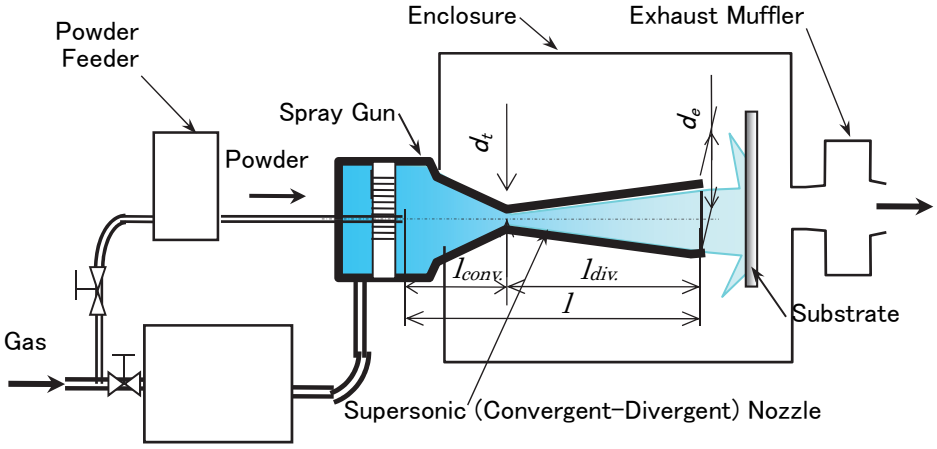

×0.65

Fig.3.22 Conceptual drawing of the cold spray equipment

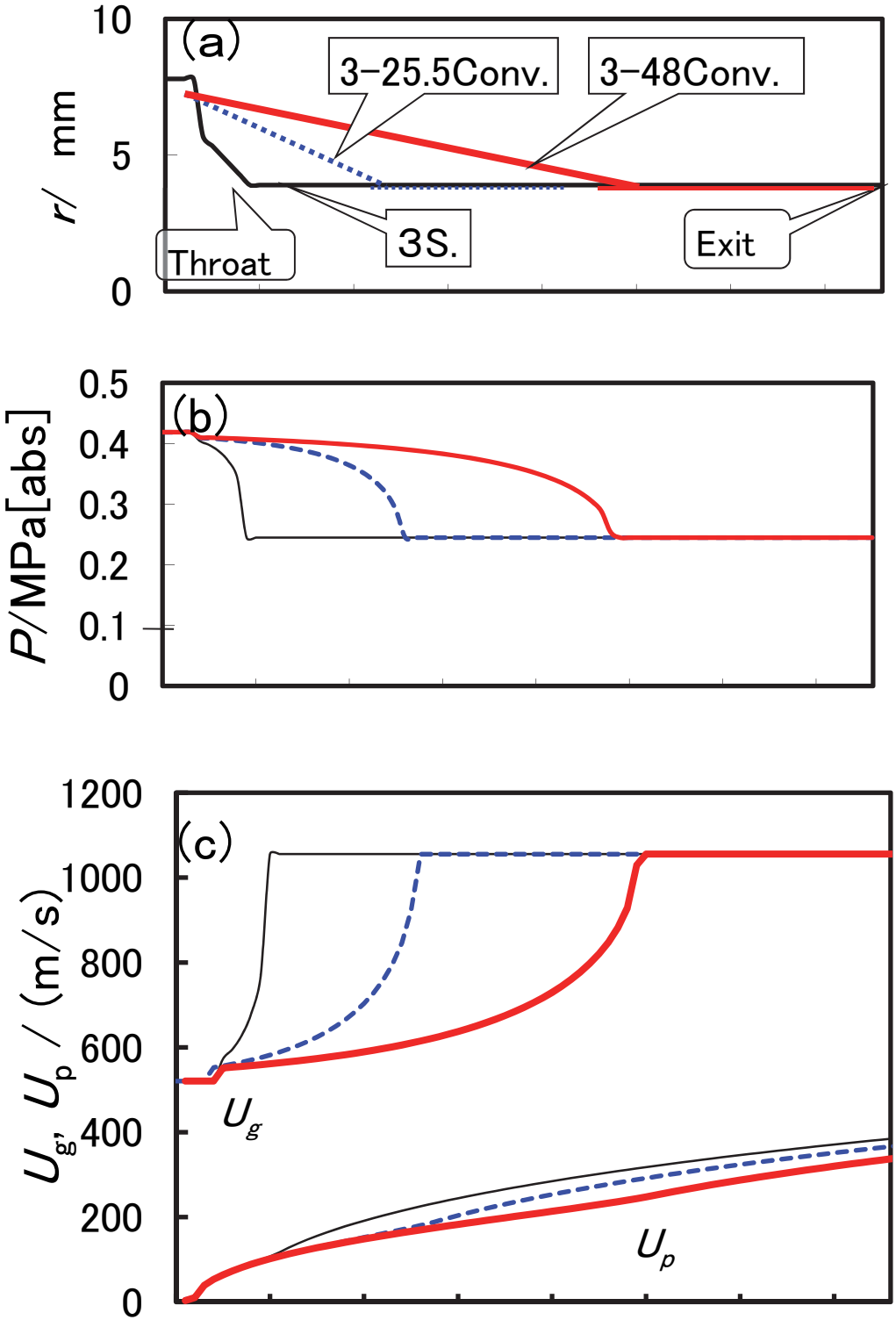
(a)
3−25.5Conv.
3−48Conv.
Throat
3S.
Exit
r/ mm
10
5
0
(b)
P/MPa[abs]
0.5
0.4
0.3
0.2
0.1
0
(c)
U_g
U_p
U_g, U_p / (m/s)
1200
1000
800
600
400
200
0

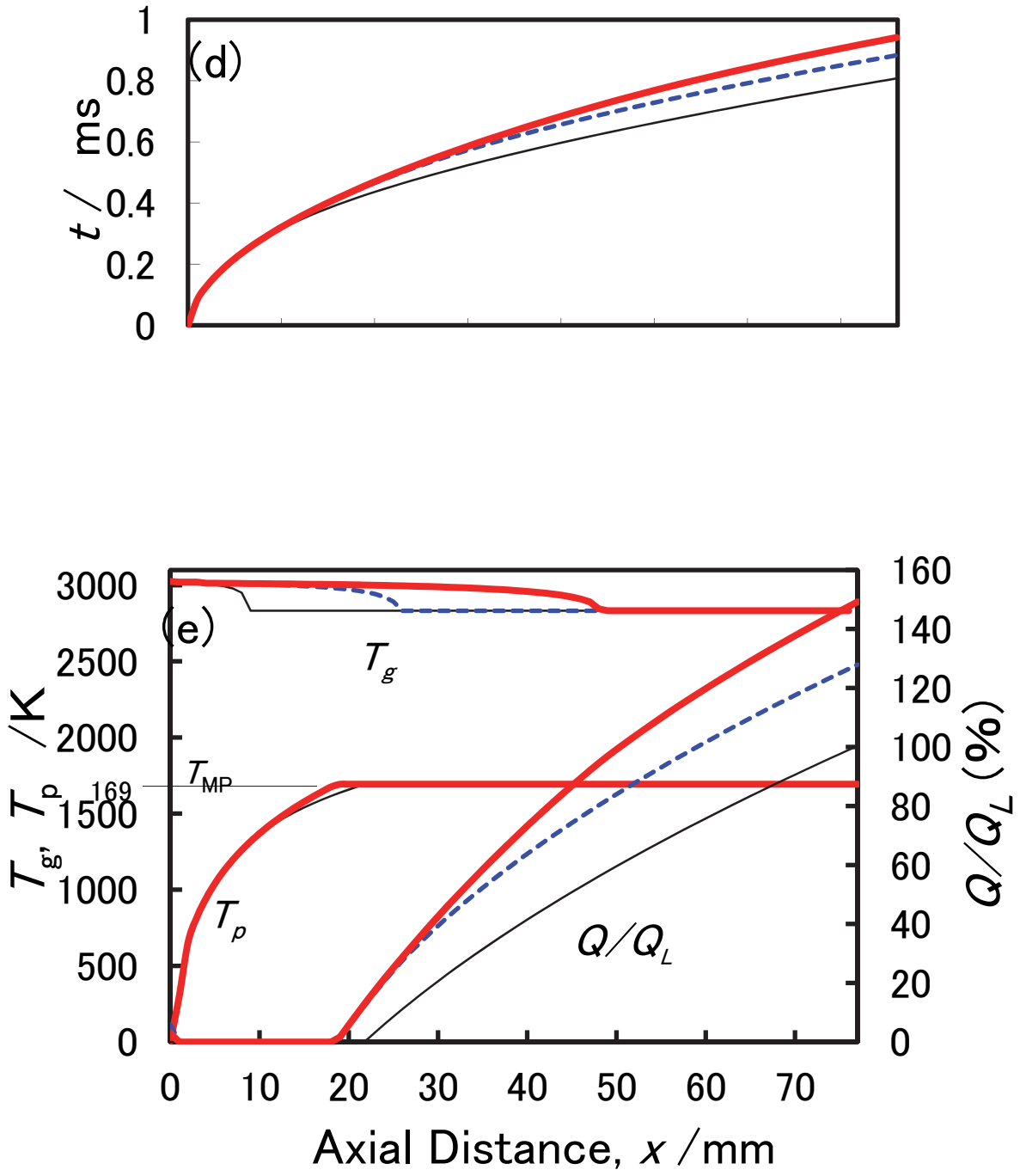

Fig.3.23 Effect of increasing in nozzle entrance convergent section length (for three nozzle shape) on calculated results of the (a) nozzle contour, (b)gas pressure, (c)velocity of gas and particle, (d)particle resident time, and (e) temperature of gas and particles and the degree of melting particle

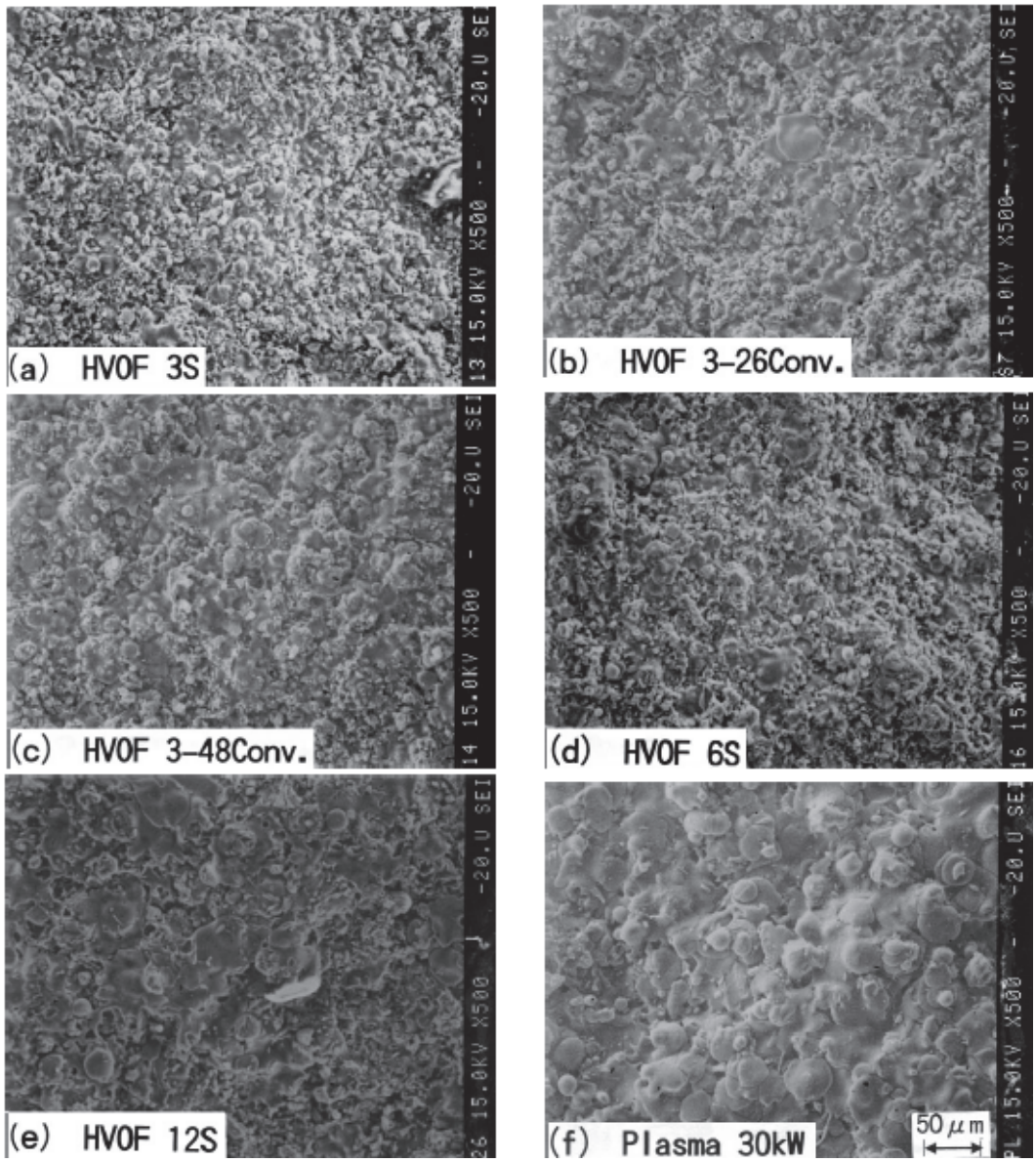

Fig.3.24 Surface SEM structures of Al_2O_3-40 mass% TiO_2 coatings sprayed by HVOF (with several nozzle shape) and plasma spraying. 3S. is 3in. straight nozzle, 3-26Conv. is 3in. converging nozzle with 26mm converging part length, 3-48Conv. is 3in. converging nozzle with 48mm converging part length, 6S. is 6in. straight nozzle, 12S. is 12in. straight nozzle

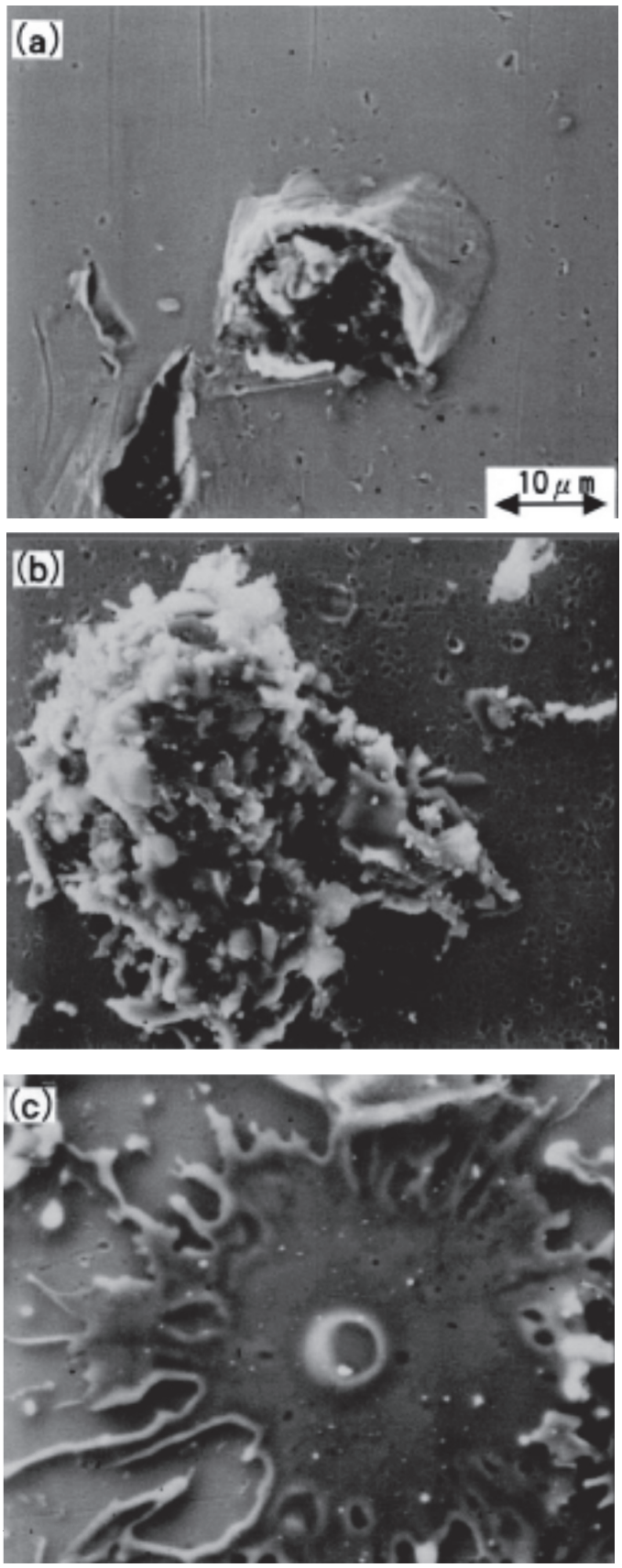

Fig.3.25 Typical patterns of the structure of Al_2O_3-40 mass% TiO_2 splats sprayed by HVOF collected on

304 stainless steel substrate: (a) of unmolten particle with trusting, (b)of semimolten particle, and (c) of molten particle with splash.

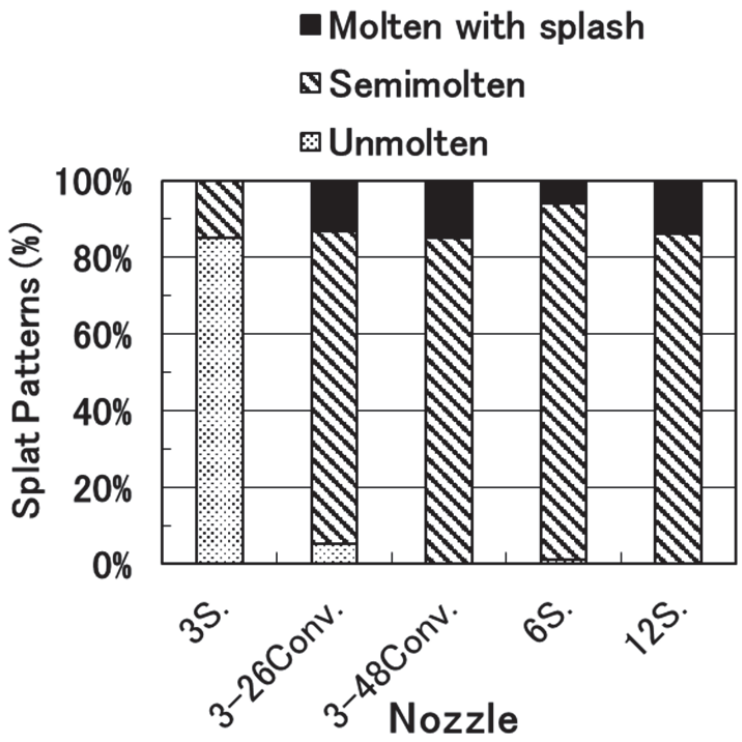

Fig.3.26 Parentage of patterns of the structure of Al_2O_3-40 mass% TiO_2 splats sprayed by HVOF with change in nozzle shape. 3S. is 3in. straight nozzle, 3-26Conv. is 3in. converging nozzle with 26mm converging part length, 3-48Conv. is 3in. converging nozzle with 48mm converging part length, 6S. is 6in. straight nozzle, 12S. is 12in. straight nozzle

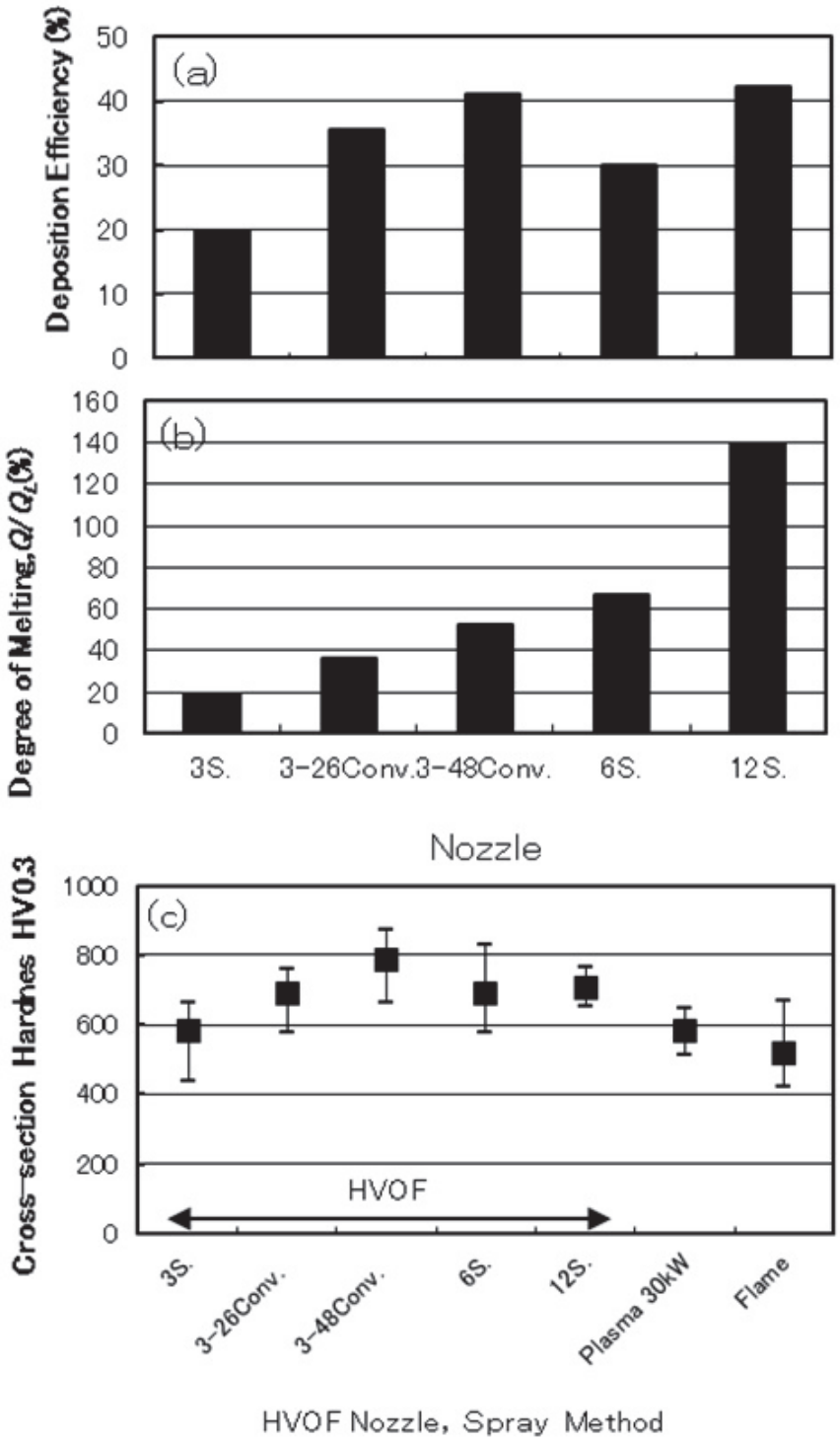

Fig.3.27 Effect of nozzle shape on (a)deposition efficiency, (b)degree of melting of particle and (c)cross-sectional hardness of sprayed Al_2O_3-40mass%TiO_2 coatings

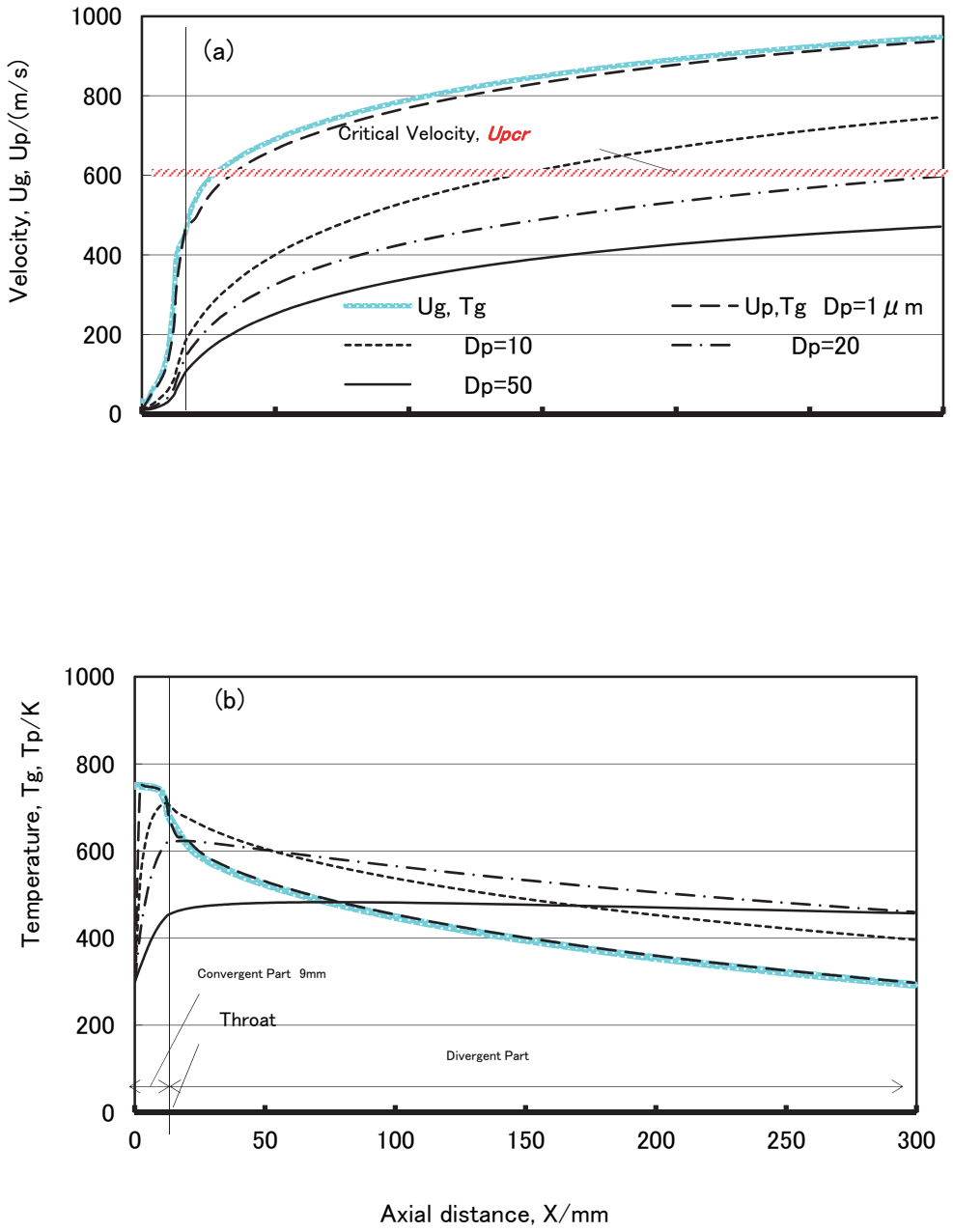

Fig.3.28 Numerical simulation results with a change in particle diameter of Ni-Al-bronze powder by cold spray: (a) velocity of gas and particle and (b) temperature of gas and particle (baseline: P_i=2MPa, U_{gi}=0m/s, T_{pi}=750K, U_{pi}=10m/s, and T_{pi}=300K)

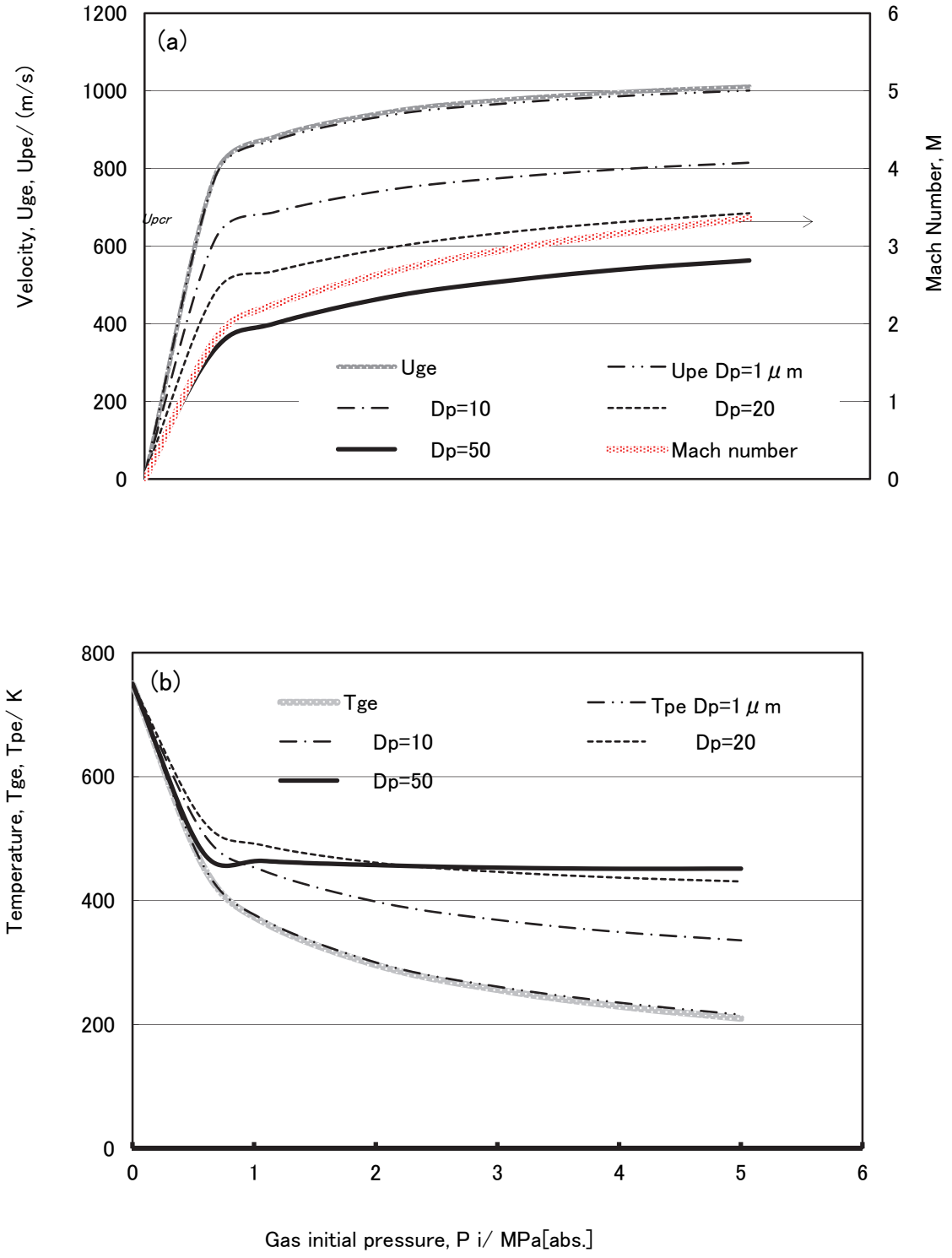

Fig.3.29 Effect of gas initial pressure on calculated results of cold spray process: (a) velocity of gas and Ni-Al bronze particle and (b) temperature of gas and particle (U_{gi}=0m/s, T_{gi}=750K, U_{pi}=10m/s, and T_{pi}=300K)

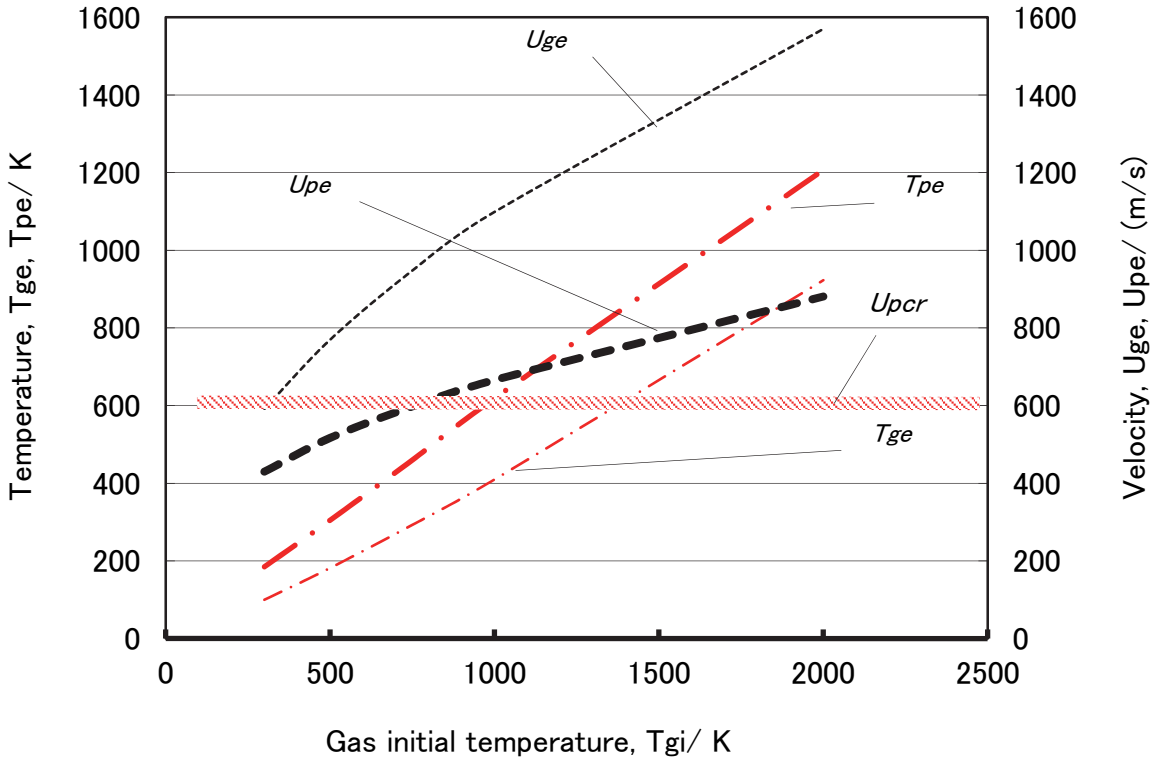

Fig.3.30 Effect of gas initial temperature on calculated results of cold spray process: velocity of gas and Ni-Al bronze particle(20 μ m), temperature of gas and particle (P_i=2MPa, U_{gi}=0m/s, U_{pi}=10m/s, and T_{pi}=300K)

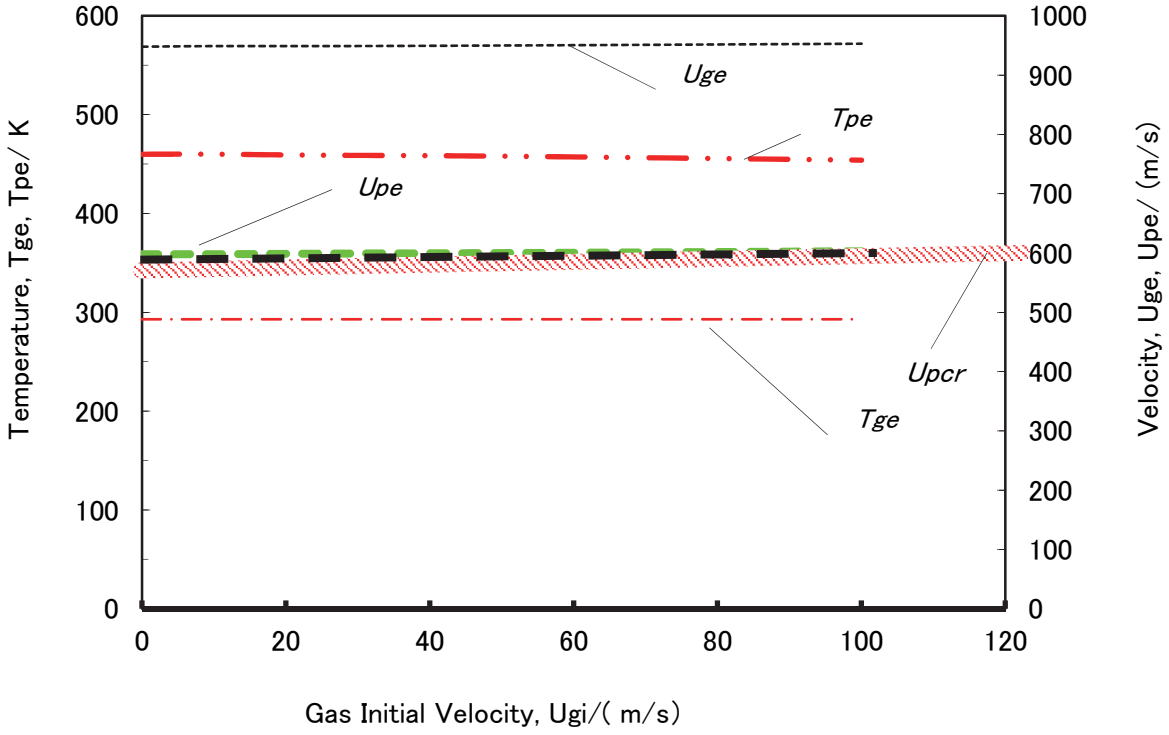

Fig.3.31 Effect of gas initial velocity on calculated results of cold spray process: velocity of gas and Ni-Al bronze particle(20 μ m), temperature of gas and particle (P_i=2MPa, T_{gi}=750K, U_{pi}=10m/s, and T_{pi}=300K)

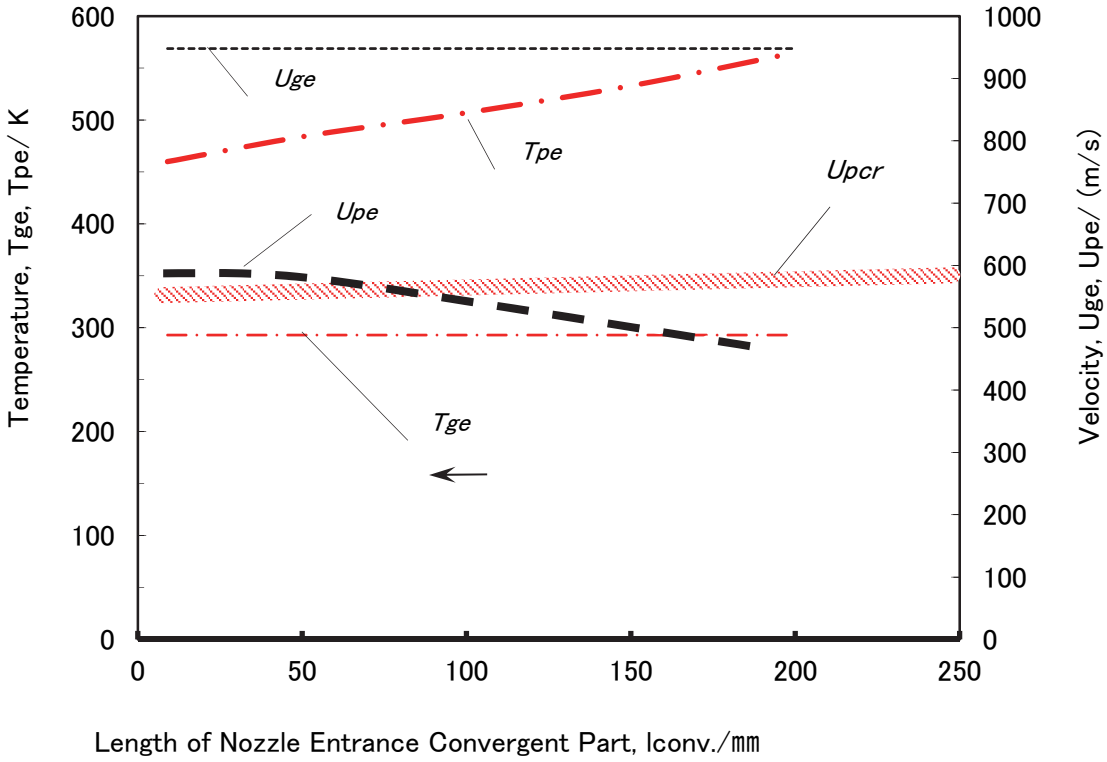

Fig.3.32 Effect of length of nozzle entrance convergent part on calculated results of cold spray process: velocity of gas and Ni-Al bronze particle(20 μ m), temperature of gas and particle (baseline: P_i=2MPa, U_{gi}=0m/s, T_{pi}=750K, U_{pi}=10m/s, and T_{pi}=300K)

Table 3.5. HVOF Spraying parameters and initial conditions

Fuel/oxygen flow rate(C_3H_6/O_2) : 90/486 L/min [normal]
Carrier gas (N_2): 35 L/min [normal]
Powder feed rate: 7.7cm^3/min
(NiCrAlY alloy: 55g/min, Al_2O_3-40mass%TiO_2: 12g/min)
Gun traverse speed: 100mm/s, Gun traverse pitch: 5mm
Spray distance: 200mm
Substrate: SUS304, SS400
<Initial conditions for numerical simulation>
Particle velocity U_{pi}: 10m/s
Particle temperature T_{pi}: 300K

Table 3.6. Shape and size of gun nozzle used and state of combustion gas stream

Nozzle	d_t mm	ϕ °	d_e mm	l mm {in}	l_i mm	l_s mm	P_i *1 MPa[abs]	P_e *2 MPa[abs]	U_{ge} *2 m/s	T_{ge} *2 K	Gas jet*3
12S7.8*4	7.8	(60)	7.8	304.8{12}	8.9	295.9	0.42	0.245	1055	2832	Weak under-expansion
6S7.8*4		(60)		156.2{6}	8.9	143.7	0.42	0.245	1055	2832	Weak under-expansion
3S7.8*4		(60)		76.2{3}	8.9	67.3	0.42	0.245	1055	2832	Under-expansion
3-26Conv.7.8		12		76.2{3}	25.5	50.7	0.42	0.245	1055	2832	Under-expansion
3-48Conv.7.8		6		76.2{3}	48.0	28.2	0.42	0.245	1055	2832	Under-expansion

*1: measured mean value, *2: calculated value *3: results of observation of HVOF free jet by photography, *4: on the market
Nomenclature d: nozzle diameter, ϕ : nozzle intake angle, l : nozzle length, P : Pressure, U : Velocity, T : Temperature,
Subscripts g : combustion gas , i : nozzle intake, t : nozzle throat, e : nozzle exit, s : nozzle straight part.

Table 3.7. HVOF spraying powder properties

Property	NiCrAlY	Al_2O_3-40mass%TiO_2
Diameter μ m	10-45(30)*	5-25(12)*
Melting point K	1727	2133
Density kg/m^3	8300	3710
Specific heat J/(kg･K)	444	1183
Latent heat of fusion $\times 10^6$J/kg	0.3	1.0

*( ): mean diameter of powder.

Table 3.8. Initial conditions of cold spray process simulation

Gas: N_2
Gas initial pressure P_i: 0.5-5.0 (2.0) MPa [abs.]
Gas initial velocity U_{gi}: 0-100 (0) m/s
Gas initial temperature T_{gi} : 300-2000 (750) K
Powder: Ni-Al Bronze
(**melting** point: 1340K, density: 7600kg/m^3,
specific heat: 440J/(kg･K), latent heat of fusion: 0.205 × 10^6J/kg)
Diameter: 1-50(20) μ m
Particle velocity U_{pi}: 0-100 (10) m/s
Particle temperature T_{pi}: 300 K

( ): baseline condition.